ORIGINAL PAPER

Wet film application techniques and their effects on the stability of RuO_2–TiO_2 coated titanium anodes

Prachi Shrivastava · Michael S. Moats

Abstract The effect of wet film application techniques on the physical and electrochemical properties and operational stability of RuO_2–TiO_2 coated titanium anodes was evaluated. Four compositions of RuO_2–TiO_2 coatings were applied to Ti substrates by three different wet coating methods—brush, dip and spin. Changing the coating technique resulted in different morphologies. Electrochemically active surface area of the coatings was related to the morphology. A shift in Ru(III)/Ru(IV) oxidation potential occurred upon changing the application technique. For lower ruthenium content coatings, this shift was related to coating lifetime. Anode stability in accelerated lifetesting showed that dip coated samples lasted up to three times longer than brush coated samples for lower ruthenium content.

Keywords Oxygen evolution · Titanium anodes · RuO_2–TiO_2 · Dip coating · Spin coating

1 Introduction

Oxygen evolution is industrially important as the counter electrode reaction for primary metal electrowinning and electroplating. Presently, most primary metal electrowinning operations use lead alloy anodes, which cause cathode impurities and exhibit high oxygen overpotentials. Coated titanium anodes hold the promise of producing higher purity deposits with less power consumption, but their cost

P. Shrivastava · M. S. Moats (✉)
University of Utah, 135S 1460E Rm 412, Salt Lake City, UT 84112, USA
e-mail: Michael.Moats@utah.edu

and long term stability have limited their commercial acceptance in primary metal electrowinning.

Coatings for titanium anodes are typically based on RuO_2 or IrO_2. RuO_2 based coatings are very stable for chlorine evolution where they exhibit lifetimes of up to 25 years, but are unstable for oxygen evolution where their life can be as short as a few days. IrO_2 based coatings are stable for oxygen evolution but have higher overpotentials and are historically more costly than RuO_2. Thus, it would be desirable to stabilize RuO_2 for oxygen evolution. Recently, an industrial demonstration of a stabilized ruthenium coated anode exhibited a life time of 3+ years in a copper electrowinning plant [1]. In addition to the long lifetime, power savings of 10% were achieved versus lead alloy anodes in the same system. The details of how RuO_2 was stabilized have not been reported. Understanding how to stabilize RuO_2 for oxygen evolution could lead to the reduced power consumption and resulting carbon footprint of metal electrowinning processes.

Traditionally, coated titanium anodes are prepared by coating the substrate with platinum group metal salt solution. The precursor solution consists of salts dissolved in a solvent, which may be organic or inorganic in nature. Then the coated substrate is dried and annealed at a higher temperature to convert the amorphous coating to a crystalline oxide. This coat-dry-anneal procedure is repeated until a desired thickness is obtained. Parameters involved during coating preparation like solvent, coating deposition, precursor solution preparation, annealing atmosphere, and temperature are known to influence the physical and electrochemical properties of the coatings [2, 3]. Oxides such as RuO_2 and IrO_2 are usually mixed with other oxides to stabilize the coatings. Along with the conducting oxides, non-conducting oxides such as TiO_2 and SnO_2 [4–8] etc. are mixed with electrocatalytic oxides. Alternative routes

Table 1 Different techniques for coating preparation

Parameter	Description	References
Additives	TiO_2, Ta_2O_5, ZrO_2, SnO_2, IrO_2	
(Binary and Tertiary)	CeO_2, Pt, Sb_2O_5, Nb_2O_5	
Application	Pulsed laser deposition	[14]
	Sputtering	[15]
	Metal organic CVD	[16–18]
	RF magnetron sputtering	[19]
	Sol–gel	[9, 20–22]
	Electrodeposition	[23–25]
	Spray pyrolysis	[26]
	Rapid thermal decomposition	[27]
	Adams fusion method	[28]
Precursor solution	Polyol method	[28]
	Pechini method—Polymeric precursor	[11, 12, 29]

for coating preparation like sol–gel [9, 10] and Pechini method [11] have been shown to improve the life of the coating as compared to the traditional method of thermal treatment. Electrodes prepared by polymeric precursor method improved the life times by five times to that of the traditional coating method [12]. Preparation of the precursor solution in isopropanol have resulted in coatings with higher life times [13]. Table 1 summarizes some of the different methods of coating deposition and additives that have been employed.

The purpose of this paper is to investigate the effect of wet coating deposition on the coating physical and electrochemical properties and correlate them to the long term stability of a coated titanium anode. Application of the wet coating is an important factor in determining the coating properties, physical as well as electrochemical. Parameters like thickness of the coating, defects, drying time, uniformity of the coating and grain size of the crystals, etc may be modulated by coating deposition. Coating deposition on a surface may depend upon the application, nature of the part to be coated, its geometry, complexity, ease of application etc. A number of coating techniques are available, some of which are mentioned in Table 1. In this paper, coatings prepared by three different wet coating application techniques viz. brush, spin and dip, are investigated. Coatings of four different RuO_2–TiO_2 compositions are analyzed for their physical and electrochemical properties as well as stability in accelerated life testing.

2 Experimental

2.1 Preparation of anodes

Samples of coated titanium anodes were prepared by applying a precursor solution to a pretreated substrate. The

samples were then processed by a traditional coat-dry-calcine method.

2.1.1 Substrate

Grade 1 titanium substrates of dimension $2.5 \times 2.5 \times 0.2$ cm were used as the support for the coating. The substrates were provided by ELTECH Systems Corporation of Fairport Harbor, Ohio, USA. Prior to coating, the substrates were grit blasted and etched at 96 °C in 18% HCl for 25 min. The substrates were then heated to 500 °C for 1 h to form a thin oxide layer over the substrate. The titanium surfaces were bluish in color indicating an approximate oxide thickness of 50 nm [30].

2.1.2 Precursor solution

Precursor solutions were prepared for four different compositions, (Ru:Ti molar ratio of 20:80, 30:70, 50:50 and 75:25). The solutions were prepared using reagent grade chemicals except for the ruthenium salt. The $RuCl_3 \cdot xH_2O$ (40% Ru) was provided by ELTECH Systems Corporation, Fairport Harbor, Ohio, USA. The other chemicals used were Titanium (IV) n-Butaoxide, 1-butanol, and HCl. The salts were dissolved in 1-butanol with 1.5% (by volume) HCl. Ruthenium concentration was kept constant at 0.3 mol dm^{-3} in every solution.

2.1.3 Wet film application

RuO_2–TiO_2 coatings were prepared by three different application techniques; dip, spin and brush coating. A RDC15 dip coater from Bungard Electroniks was used to prepare the dip samples. Titanium substrates were attached to a titanium rod by spot welding for dip coating. The substrate was then fully immersed into the precursor

solution and withdrawn at a constant rate of 0.18 m min^{-1}. Spin coated samples were prepared by using a Laurells WS-400A-6NPP/LITE single wafer spin coater. The substrate was held onto the spinning chuck by vacuum. 0.2 mL of precursor solution was applied to the substrate using an adjustable volume pipette and the sample was spun at 500 rpm for 15 s. Brushed samples were prepared because of their ease of preparation and comparison with dip and spin coated samples and most prior literature.

2.1.4 Electrode preparation

After the precursor solution was applied to the pre-treated titanium substrate, the wet coating was allowed to dry in air until the part was visibly dry. Following drying, a high temperature calcination of the parts occurred at 470 °C for 10 min. This coat-dry-calcine procedure was repeated until the total oxide loading was 2.2 mg cm^{-2} for each method. The number of coats varied from 4 to 9 coats for brush, 6 to 14 for spin and 8 to 18 for dip coating. The required number of coats increased with decreasing titanium content. After achieving the desired weight, the samples were calcined at the same temperature for 1 h. Three samples for each composition and application technique were prepared for reproducibility.

Brush and spin coated samples were coated on one side whereas the dip coated samples were coated on both sides. One of the sides was ground off for dip coated samples prior to characterization. The amount of coating on either side of the dip coated sample were approximately the same ±0–20% as determined by X-ray fluorescence.

2.2 Physical characterization

2.2.1 X-Ray Diffraction (XRD)

A Siemens X-Ray D 5000 Diffractometer was used for microstructural analysis of the coating. A single crystal NiSi crystal was used for peak broadening correction due to instrumental errors. XRD was run from 10° to 100° at a step size of 0.020° and step time of 0.4 s at room temperature.

2.2.2 Scanning Electron Microscopy (SEM)

The effect of the wet coating application on the coating morphology was analyzed by scanning electron microscopy. Most SEM was performed on a Hitachi S-3000 N system equipped with X-ray Energy Dispersive Spectroscopy. The samples were analyzed at a potential of 20 kV. High resolution SEM was performed using Hitachi S-4500 equipment.

2.2.3 X-Ray Fluorescence (XRF)

XRF was performed on a Jordan Valley—Analytical Products (JVAR) Model EX3600 system. The amount of ruthenium present in fresh and failed sample was measured by comparing net intensities produced by XRF.

2.3 Electrochemical characterization

The electrochemical properties were characterized by cyclic voltammetry and polarization experiments conducted using a Gamry PCI4-750 Potentiostat installed on a Dell PC operated using software provided by Gamry. The experiments were performed at room temperature in 0.5 M H$_2$SO$_4$ vs. saturated Ag/AgCl reference electrode. Coated anodes were attached to a titanium rod by spot welding and used as the working electrode.

2.3.1 Cyclic voltammetry

Cyclic voltammetry experiments were performed in a three-compartment cell with a glass frit and a Luggin capillary. Platinum wire of 0.61 mm diameter was used as a counter electrode. It was immersed up to 2.5 cm in the electrolyte during each experiment. Potential was scanned from 0.2 V to 1.1 V vs. Ag/AgCl at various scan rates. The distance between the Luggin and anode was maintained at 2.5 cm.

2.3.2 Linear sweep voltammetry

Tafel experiments were performed to analyze the activity and overpotential of the coatings prepared by different methods. A single chambered cell was used for the experiment with a 2.5 × 2.5 cm^2 zirconium counter electrode. Working and counter electrodes were attached to titanium rods. Distance between the reference and working was maintained from 4 to 5 cm. Potential was swept from 1.0 to 1.6 V vs. Ag/AgCl at a rate of 0.1 mV s^{-1}.

2.3.3 Electrochemical Impedance Spectroscopy (EIS)

EIS was performed on fresh and failed samples in a setup similar to cyclic voltammetry experiments. The experiments were run in potentiostatic mode at a potential of 0.6 V vs. Ag/AgCl. Frequency was varied from 100,000 Hz to 10 MHz at a rate of 10 point per decade.

2.4 Stability testing

The stability of coated anodes was tested by subjecting each sample to life tests under accelerated conditions. A current density of 10 kA m^{-2} was applied to a single

component cell using a Sorensons model number DCS33-33E power supply. The experiments were run in 1.5 M H_2SO_4 at 50 °C. A 2.5 × 2.5 cm^2 zirconium cathode was used as the counter electrode. Cell voltage was monitored throughout the experiment using a National Instruments data acquisition card USB9201 on a VI logger installed in a standard PC computer.

3 Results and discussion

3.1 Morphology and microstructure

Figure 1a–i are SEM images for the brush, spin and dip coatings for three different coating compositions. The morphology as observed in Fig. 1 can be described in terms of low and high ruthenium content. For lower ruthenium content (20–30 mole%), coatings produced by brushing give rise to a traditional mud cracked structure. These cracks are present throughout the surface. On the other hand, spin and dip coated samples exhibited cracks that are less dense and wide. On increasing the ruthenium content to 30 mole% and 50 mole%, a decrease in nature of the

cracks in terms of the density and width is prominent for all the techniques. The 70 mole% ruthenium coating morphology was similar to the 50% mole coating morphology. For higher ruthenium content, the coating morphology appears to be less dependent on the preparation technique as observed in Fig. 1g–i. A decrease in the cracks and pore sizes is seen which is similar to results reported by Kameyana et al. [31] and contradictory to the results reported by [6]. The difference in the results may be attributed to the differences in the thickness of the coating and/or preparation conditions.

Non-homogeneous coatings are obtained at lower ruthenium concentrations by dip and spin techniques as opposed to homogeneous brush coatings. Small agglomerates can be seen in dip and spin coatings and their density increases with the ruthenium content in the coating. These crystallites start to appear in brushed samples at higher ruthenium content.

A closer examination of these agglomerates indicates clusters of small crystals as seen in Fig. 2. From the Electron Dispersion Spectroscopy (EDX) data obtained from spots 1 and 2 in Fig. 2, these agglomerates appear to be enriched in ruthenium. The presence of such crystallites has been reported earlier by other groups for different
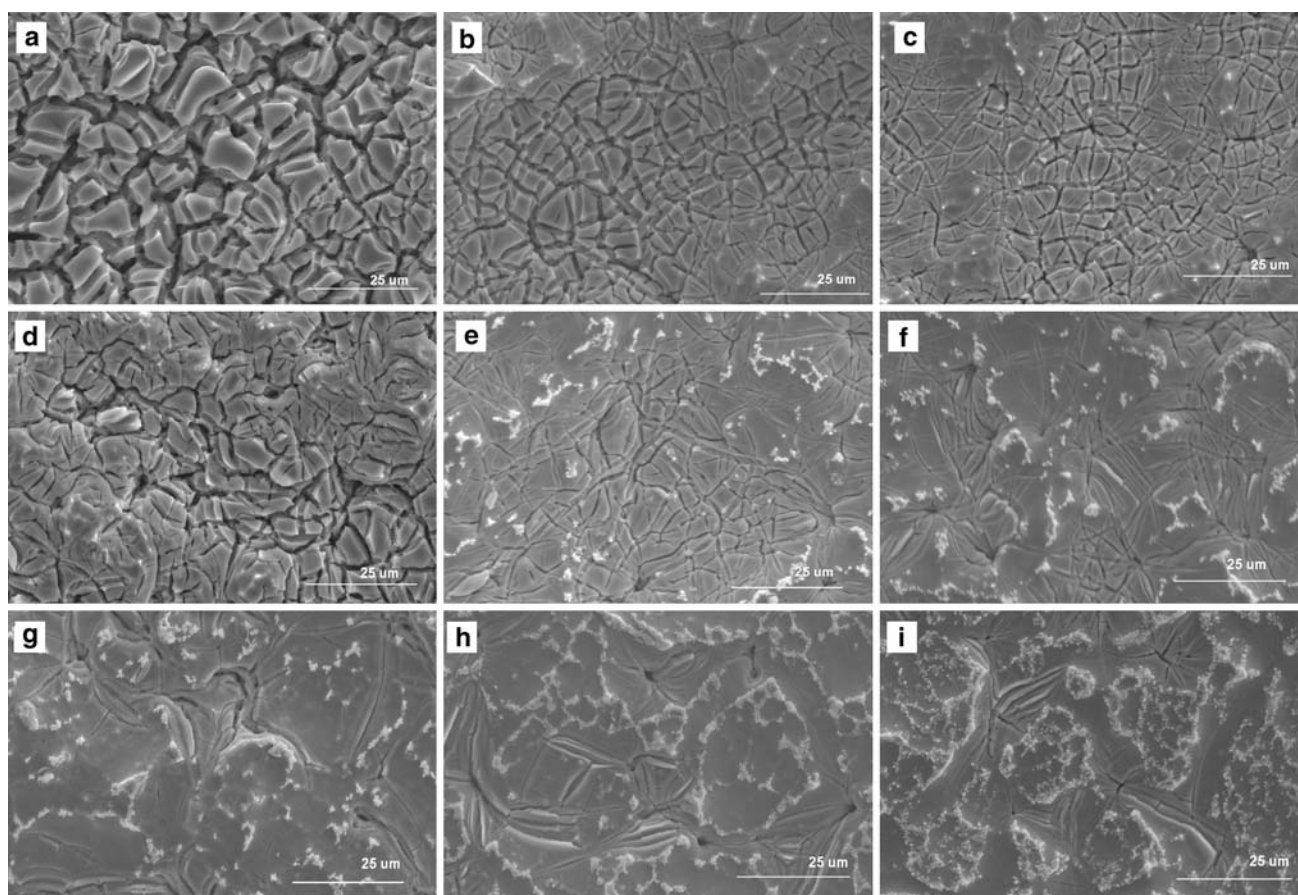
Fig. 1 SEM images of the surfaces of $RuO_2(20)$–$TiO_2(80)$—(**a**) brush (**b**) spin (**c**) dip; $RuO_2(30)$–$TiO_2(70)$-(**d**) brush (**e**) spin (**f**) dip; $RuO_2(50)$–$TiO_2(50)$-(**g**) brush (**h**) spin (**i**) dip coated titanium anodes
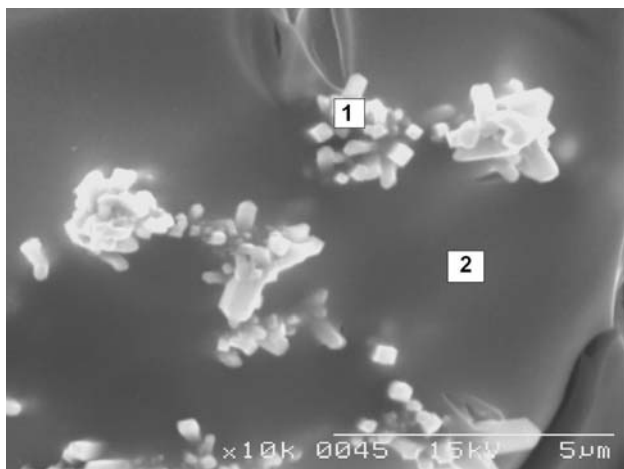
Fig. 2 SEM image of crystallites on dip coated Ru(30)–Ti(70) sample
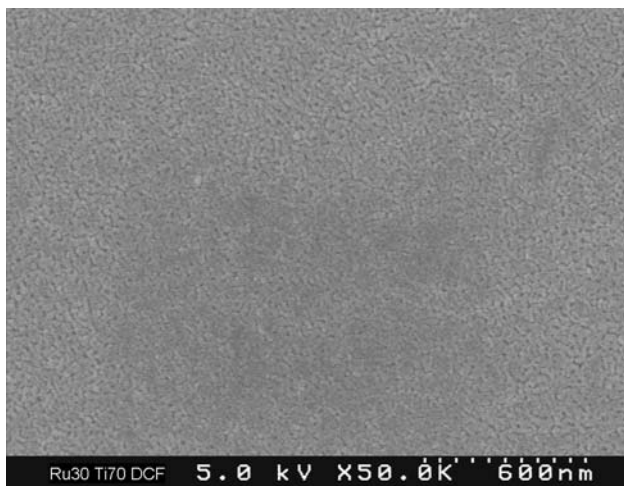

Fig. 3 High magnification SEM image of the surface of a dip coated Ru(30)–Ti(70) sample

coating preparations and for binary as well as tertiary oxides [32–34].

The nanostructure of the coating was analyzed by high magnification scanning electron microscopy. The surface reveals a nanoporous structure with nanocrystalline features as seen in Fig. 3. It is observed that the nanostructure of the coating is independent of the deposition method in this study. This inference is further strengthened by the XRD where the coating deposition technique does not have an appreciable affect on the grain size. The grain size for all the coatings are 14–19 nm, which lies in the same range as reported by another group [35].

3.2 Surface area and electrochemical activity

A typical voltammogram for the three coating types is shown in Fig. 4 for $RuO_2(20)$–$TiO_2(80)$ at a scan rate of
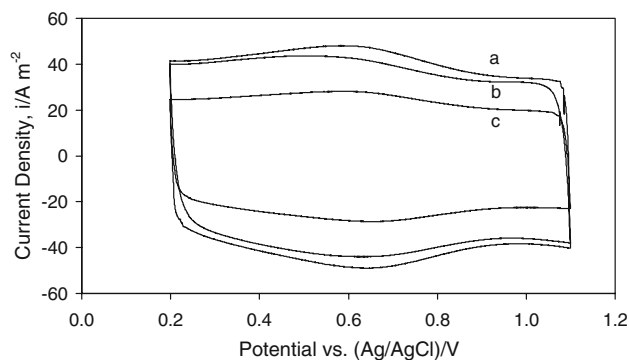
Fig. 4 Cyclic voltametric curve for (a) dip (b) brush and (c) spin coated samples showing shift in the oxidation peak potential for $RuO_2(20)$–$TiO_2(80)$. Experimental conditions: scan rate 100 mV s^{-1}, 0.5 M H_2SO_4, Ag/AgCl reference electrode, Pt wire counter electrode, room temperature

100 mV s^{-1}. The voltammograms show a broad peak that result from the reversible oxidation and reduction of the surface Ru atoms. Ruthenium undergoes a state change of Ru(III) → Ru(IV) at 0.4 V vs. NHE [36] as given by the equation:

$$RuO_x(OH)_y + \delta H^+ + \delta e^- \leftrightarrow RuO_{x-\delta}(OH)_{y+\delta} \qquad (1)$$
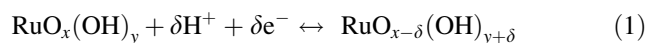
The voltammograms for brush, spin and dip are similar in shape except that a small shift in the oxidation peak potential is observed. The peak potential for the dip coating is higher than spin which in turn is higher than the brush coating. This is prominently seen for coatings with lower ruthenium content, Ru (20 mole% and 30 mole%). Variation in the oxidation peak potential as a function of ruthenium concentration and deposition technique is shown in Fig. 5. Much smaller values of the oxidation peak potentials were obtained for higher ruthenium content coatings. A similar shift was reported previously by Kotz
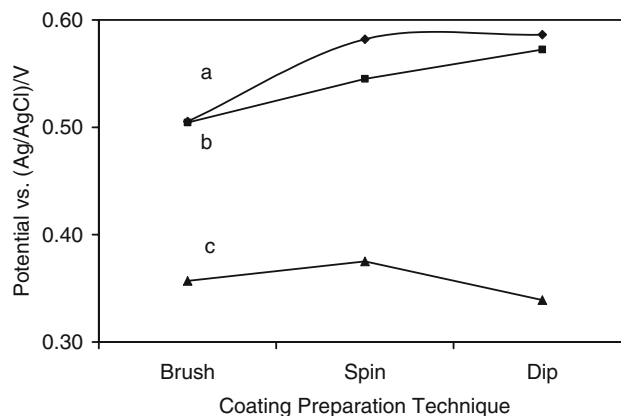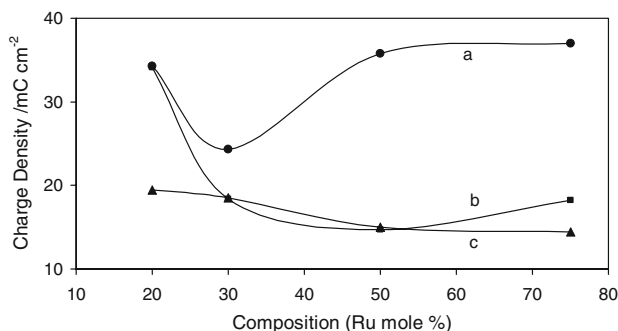

Fig. 5 Variation in the oxidation peak potential as a function of coating deposition technique for (a) $RuO_2(20)$–$TiO_2(80)$, (b) $RuO_2(30)$–$TiO_2(70)$ and (c) $RuO_2(50)$–$TiO_2(50)$ Experimental conditions: Scan rate 100 mV s^{-1}, 0.5 M H_2SO_4, Ag/AgCl reference, Pt wire counter electrode, room temperature

and Stucki for RuO_2–IrO_2 coatings but was related to the Ir content of the coating [15].

The shift in oxidation potential clearly varies with the morphology of the coating. Compact coatings are obtained by dip and spin coating techniques and they have a higher oxidation potential. Since the oxidation of the ruthenium involves the insertion of protons and the diffusion of said species, it is believed that the shift in oxidation potential based on coating morphology is related to the ease of insertion or diffusion of these species. In more compact coatings, it appears to be more difficult to insert protons and/or diffusion is inhibited. This explanation is speculative and this effect is still being investigated.

Charge obtained from the cyclic voltammetric curves is an indication of the electrochemically active sites present at the surface of the coating. The voltammetric charge was determined by integration in the potential range 0.2–1.1 V vs. Ag/AgCl. Figure 6 shows the charges obtained for the brush spin and dip samples for varying ruthenium concentrations. It is seen that brush coated samples have higher charge throughout the composition range which correlates to its more defective/cracked microstructure. Charges obtained for dip coated samples decreases with concentration whereas charges obtained from spin coated samples were lowest and they did not vary much over the concentration range. It is clear from these charges that more electrochemically active sites are present and a large surface area is available for the more cracked structure (brush coating).

Polarization experiments were conducted to analyze the effect of wet coating deposition on activity of the coating. Figure 7 shows the Tafel plot for brushed $RuO_2(20)$–$TiO_2(80)$ coating. A similar shaped plot is obtained for all the samples. An increase in the Tafel slope observed at higher overpotential has also been reported previously [37, 38]. This increase in the slope results from the blocking of pores
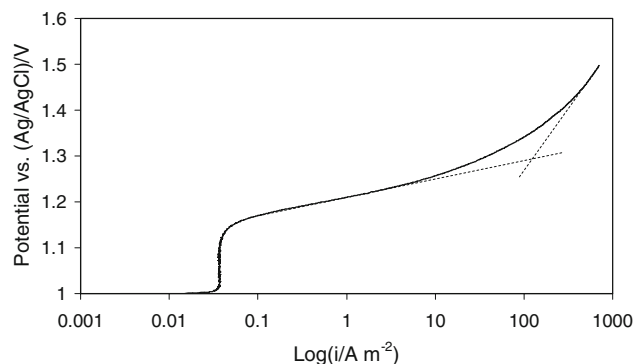
Fig. 7 Tafel plot showing the increasing Tafel slope at higher overpotential for $RuO_2(20)$–$TiO_2(80)$ Experimental conditions: 0.1 mV s^{-1} scan rate, 0.5 M H_2SO_4, Ag/AgCl reference, Zirconium counter electrode, room temperature

Table 2 The effect of coating composition and application technique on Tafel slopes (Potential vs. (Ag/AgCl)/V decade^{-1}) at high current density in 0.5 M H_2SO_4
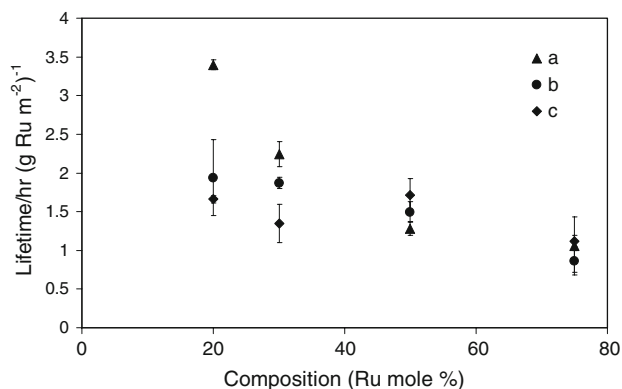
Composition	Brush	Spin	Dip
Ru(20)–Ti(80)	0.292	0.245	0.198
Ru(30)–Ti(70)	0.287	0.230	0.157
Ru(50)–Ti(50)	0.229	0.194	0.183
Ru(75)–Ti(25)	0.197	0.204	0.175

due to oxygen evolution or change in the mechanism of oxygen evolution as has been suggested previously [3]. Tafel slopes at higher potential, 1.4–1.5 V vs. Ag/AgCl, which are more indicative of conditions seen in industrial electrolysis, are tabulated in Table 2. Tafel slopes for brushed samples vary inversely with ruthenium content; that has also been reported previously [39]. Tafel slopes for all the samples are slightly higher than the values reported in literature. This may be attributed to the uncompensated ohmic drop in the solution or to the use of larger sized anodes.

3.3 Stability

Stability of an anode is defined in this paper as the ability to operate at a constant current without a significant increase in potential. Near the end of an anode life, a rapid increase in its potential is observed. The rapid increase in potential is due to the presence of an additional resistance that builds up gradually, either due to the loss of active material present in the coating or due to formation of a non-conducting layer. The insulating layer can be caused by either a surface deposit or the growth of a non-conductive oxide between the substrate and the coating. Stability is tested by performing life tests at accelerated conditions, such as 10 kA m^{-2} at 50 °C in 1.5 M H_2SO_4.

Accelerated life testing shows that dip and spin coated samples respond better than the brushed samples in terms

Fig. 6 Charge obtained from cyclic voltammograms for (a) brush (b) dip and (c) spin coatings as a function of composition. Experimental conditions: Potential range vs. Ag/AgCl 0.2–1.1 V, scan rate 100 mV s^{-1}, 0.5 M H_2SO_4, platinum counter electrode, room temperature
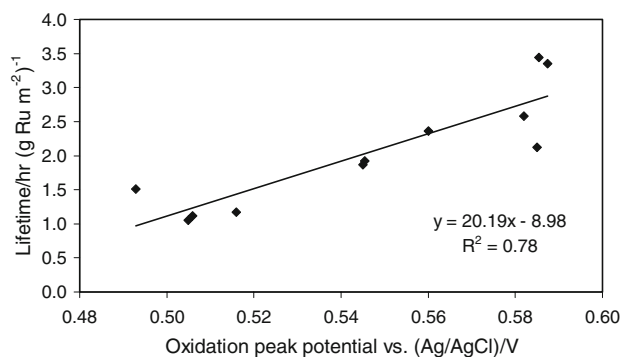
Fig. 8 Life time of the coating in terms of Ruthenium concentration (a) dip (b) spin (c) brush. Accelerated life test conditions: 1.5 M H_2SO_4, 50 °C and 10 kA m^{-2}, Zirconium cathode

Fig. 10 Potentiostatic EIS for $RuO_2(20)$–$TiO_2(80)$ fresh (a) dip (b) brush and failed (c) brush and (d) dip samples, 0.5 M H_2SO_4, 0.6 V, Ag/AgCl reference, Pt wire counter electrode, room temperature
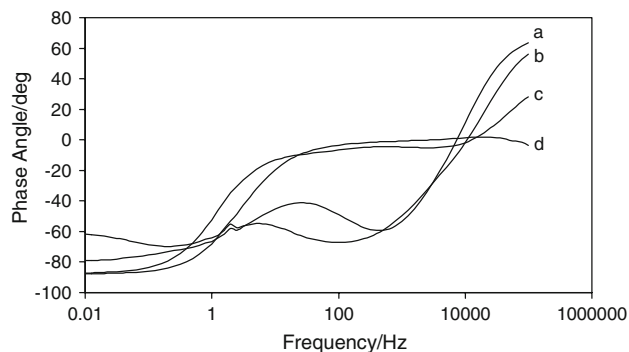
of overall life time at lower ruthenium contents and reproducibility at all compositions as shown in Fig. 8. For low ruthenium contents, preparation of the coatings by dipping was effective in improving the life time. The life of the samples is doubled for Ru 30 mole% and tripled for Ru 20 mole% compared to brushed samples. However, for higher ruthenium contents the life of the coating is independent of the preparation technique.

On comparing the data presented in Figs. 5 and 8, the oxidation potential for Ru (III)/Ru (IV) shifts to a higher value for dip coated samples, which also last longer. The correlation between the oxidation potential and anode stability for lower Ru content samples (Ru 20 and 30 mole%) is shown in Fig. 9.

A change in the color of the electrolyte was observed during the life tests, indicating a loss of ruthenium from the coating. This was confirmed by performing X-ray fluorescence on fresh and failed brush and dip coated samples. XRF indicated that 40–50% of the precious metal was lost during the lifetests, meaning 50–60% of the original ruthenium

Fig. 9 Oxidation Potential vs. Coating stability for $RuO_2(20)$–$TiO_2(80)$ and $RuO_2(30)$–$TiO_2(70)$ brush, spin and dip coatings. Accelerated Life test conditions: 1.5 M H_2SO_4, 50 °C and 10 kA m^{-2}, Zirconium cathode

remained on the failed life tested sample irrespective of the coating application technique. This leads to the inference that although some wear of the coating occurred, it was not the major anode failure mechanism in these tests. In addition to wear, coating failure can occur due to formation of an insulating layer i.e. passivation and/or deposition of other impurities. The deposition of impurities was absent in these experiments. Thus the formation of a passivating TiO_2 layer was the most likely cause of failure.

To confirm that passivation was the major failure mechanism, electrochemical impedance spectroscopy experiments were conducted on fresh and failed samples. These results are shown in Fig. 10 as a Bode plot. A high frequency peak for the failed sample is observed which provides an indication of the formation of a passive layer presumably TiO_2 [40, 41].

Table 3 summarizes all the electrochemical, physical and stability measurements of the coated titanium samples tested. It has been shown that the dip coating can improve the life time of an anode by as much as 3 times compared to brushing. However, as shown in Table 3 dip coated samples were prepared with more coats than the brush coated samples. It has been previously shown that life of the coating improves on increasing the number of coats and then attains saturation [42]. To evaluate if the difference lays between the number of coats or the wet film technique, brush coated samples with 9–11 coats of Ru(20)–Ti(80) and Ru(30)–Ti(70) coatings with similar loadings were prepared and subjected to life testing. An example of the results from brushed and dipped coated samples with the same number of coats and similar loadings are presented in Fig. 11. The life of the brushed samples did increase up to 20% with an increase in the number of coats. Dip coated samples, however, still exhibited a significantly longer life as compared to brushed samples with the same number of coats.

From Table 3, it is seen that deposition technique influences the physical and electrochemical properties of

Table 3 Comparison of electrochemical and morphological properties for all brush dip and spin coated samples

Samples	Ru(20)–Ti(80)			Ru(30)–Ti(70)			Ru(50)–Ti(50)		
Properties	Brush	Spin	Dip	Brush	Spin	Dip	Brush	Spin	Dip
Number of coats	4–5	6–7	9	5	8	11–12	7	14	18
Grain size/Å	139	165	160	181	190	183	192	179	171
Electrocatalytic charge/q cm^{-2}	34	19	34	24	19	18	36	15	15
Oxidation potential III/IV Potential vs. (Ag/AgCl)/V	0.505	0.582	0.586	0.504	0.545	0.573	0.357	0.375	0.339
Tafel slope, Potential vs. (Ag/AgCl)/V dec^{-1}	0.292	0.246	0.198	0.287	0.230	0.157	0.229	0.194	0.180
Stability/h (gm Ru m^{-2})$^{-1}$	1.2	1.9	3.4	1.3	1.8	2.2	1.7	1.5	1.3
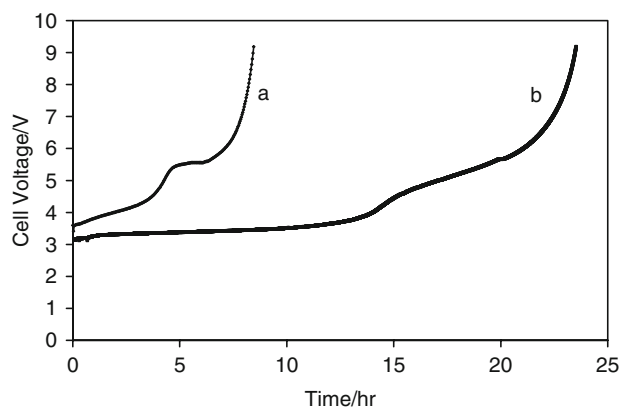
Fig. 11 Example of accelerated lifetest data from RuO$_2$(20)–TiO$_2$(80) (a) brush and (b) dip coated samples with nine coats each. Accelerated life tests, 1.5 M H$_2$SO$_4$, 50 °C, 10 kA m^{-2}, Zirconium cathode

the coatings and the stability of the coated anode. It is believed that the application method affected the coating by changing the wet film thickness and the drying characteristics. Thicker wet films applied per coat may have resulted in trapped solvent, which was still present within the internal structure of the coating after the air drying used with these samples. This would lead to higher mechanical stresses during drying and annealing resulting in the formation of a more-cracked morphology (e.g. brushed samples). Thinner coats produced a less stressed coating and hence a less cracked coating (e.g. spin and dip samples). Even when brush samples were produced with the same number of coats as the dip samples, the morphology was still more cracked. This indicates that higher mechanical stresses were developed during brushing than dipping, but the exact mechanism involved is not fully understood. The more cracked coating of the brush samples appears to process a higher surface area as determined by surface charge measurements. Interesting, the higher surface area of brushed samples did not translate into a lower Tafel slope at higher current densities as compared to dip and spin samples. If the increase in Tafel slope at higher current densities is caused by gas bubble blinding [42],

then a cracked surface may trap more bubbles than a smoother surface. Thus a smoother surface may actually process a higher active surface area during gas evolution which could explain the lower Tafel slopes of dip and spin coatings at higher current densities.

It is believed that two aspects of the coatings produced by different wet film application techniques affected anode stability. These are the surface morphology and the shift in ruthenium oxidation potential. Based on the failure analysis of the samples, the main failure mechanism was passivation. It is widely believed that the passivation layer occurs between the coating and titanium substrate. The passivation layer is a non-conductive oxide presumably formed by the oxidation of titanium by water as represented by Eq. 2

$$TiO_{2-x} + xH_2O = TiO_2 + 2H^+ + 2e^- \qquad (2)$$
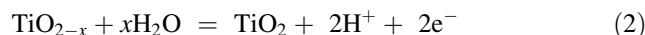
The rate of water penetration through the coating to the substrate would thus affect the stability/passivation of the coated anode. The rate of the water penetration would be affected by the coating morphology and the coating thickness similar to diffusion through a porous structure. A coating with more cracks would seem to be more accessible to water penetration and thus easier to passivate (e.g. brush samples have a shorter lifetime than dip or spin samples).

While this explanation fits the results observed, it is not believed to be the entire effect. High resolution SEM images indicate that all of the coatings in this study exhibit 20–30 nm nanopores. These pores would be sufficiently large to allow the penetration of water regardless of the crack structure of the coating. Thus, it is believed that the thickness of the coating (e.g. tortuous path length) is probably involved with water passing through the nanopores. Cracks would reduce the effective path length that water molecules have to travel to reach the substrate and thus could still affect anode stability.

Titanium substrates in this study were pre-oxidized in air to form a thin layer of titanium oxide. In another paper from our group [43], it is clearly indicated that life of the anode can be significantly improved by the presence of a thin oxide layer. It is believed that a semiconducting oxide,

TiO_x, is formed, which improves the stability of the coating, as opposed to an insulating oxide. It is believed that a semiconducting matrix of Ru–Ti–O_x, is formed at the coating substrate interface which prolongs the passivation of the coating. A detailed analysis of this is still under investigation.

The final aspect of coating thickness has to due with the dissolution of the coating. In all of the tests, 50–60% of the RuO_2–TiO_2 coating remained at failure. This would mean that the dissolution (or wear) rate of the dip samples were $2\times$–$3\times$ slower than brush samples at the lower ruthenium contents. The slower wear rate would result in a thicker coating for a longer duration of the accelerated life test. The thicker coating would have a longer effective path length and thus retard passivation.

The transition of pure ruthenium oxide from lower to higher oxidation states, i.e. from RuO_2 to RuO_4 occurs at 1.4 V vs. NHE leading to formation of unstable oxides [39]. During accelerated life testing at 10 kA m^{-2}, the anode potential is higher than 1.4 V vs. NHE. This would indicate that RuO_4 would form and the ruthenium content of the coating would dissolve. It is believed that the shift in the oxidation peak potential of Ru(III) to Ru(IV) to a higher potential, which is seen in case of dip and spin coating, could be indicative of an increase in the potential at which unstable higher oxides of ruthenium are formed for dip coated samples. If this were true, this would explain the slower down the dissolution rate of the dip and spin samples. The fundamental cause for the shift in the oxidation potential resulting from changes in wet film application technique is not fully understood and should be the subject of additional research.

Combining all of these aspects, wet film application techniques appears to affect coating stability by retarding substrate passivation. The inhibiting of passivation appears to be caused by increasing the effective path length of water penetration through the coating by changing the cracked morphology of the coating and slowing down the dissolution rate of the coating.

4 Conclusions

Wet coating deposition methods can alter the physical and electrochemical properties of RuO_2–TiO_2 coatings. These changes in properties result in a change in the stability of coated titanium anodes. Dip and spin coated samples of lower ruthenium content were found to be superior to brush coated samples in terms of life. It is believed that the life time differences result from changes in surface morphology (cracking) and coating wear rate (ruthenium oxidation).

References

1. Moats M, Brown C, Hardee K (2006) In: Kellar J (ed) Functional fillers and nanoscale minerals II, SME, Littleton, Colorado
2. Yang L, Farr J, Ashworth M (2000) Trans Inst Met Finish 78(3):96
3. Trasatti S (ed) (1980) Electrodes of conductive metallic oxides: Part A. Elsevier Amsterdam
4. Boodts J, Trasatti S (1990) J Electrochem Soc 137(12):3784
5. Gaudet J, Taveres A, Trasatti S et al (2005) Chem Mater 17:1570
6. Makarychev Y, Spasskaya E, Khodkevich S et al (1976) Elektrokhimiya 12(6):994
7. Nanni L, Polizzi S, Benedetti A et al (1999) J Electrochem Soc 146(1):220
8. Silva L, Alves V, Silva A et al (1997) Electrochim Acta 42(2):271
9. Panic V, Dekanski A, Milonjic S et al (1999) Colloids Surf A 157:269
10. Panic V, Dekanski A, Miskovic-Stankovic V et al (2005) J Electroanal Chem 579:67
11. Oliveira-Sousa A, Silva M, Machado S et al (2000) Electrochim Acta 45:4467
12. Forti J, Olivi P, Andrade A (2001) Electrochim Acta 47:913
13. Coteriro R, Teruel F, Ribeiro J et al (2006) J Braz Chem Soc 17(4):771
14. Hiratani M, Matsui Y, Imagawa K et al (2000) Thin Solid Films 366:102
15. Kotz R, Stucki S (1986) Electrochim Acta 31(10):1311
16. Shin W, Yoon S (1997) J Electrochem Soc 144(3):1055
17. Green M, Gross M, Papa L et al (1985) J Electrochem Soc 132(11):2677
18. Si J, Desu S (1993) J Mater Res 8:2644
19. Battaglin G, Rigato V, Zandolin S et al (2004) Chem Mater 16:946
20. Aparicio M, Klein L (2004) J Sol–Gel Sci Technol 29:81
21. Armelao L, Barreca D, Moraru B (2003) J Non Cryst Solids 316:364
22. Takasu Y, Onoue S, Kameyama K et al (1994) Electrochim Acta 39(13):1993
23. Metikos-Hukvic M, Babic R, Jovic F et al (2006) Electrochim Acta 51:1157
24. Hadzi-Jordanov S, Angerstein-Kozlowska H, Vukovic M et al (1978) J Electrochem Soc 125:1471
25. Briss V, Myers R, Angerstein-Kozlowska H et al (1984) J Electrochem Soc 131:1502
26. Fernandez J, Chialvo M, Chialvo A (1997) J Appl Electrochem 27:1323
27. Foti G, Mousty C, Reid V et al (1998) Electrochim Acta 44:813
28. Marshall A, Borresen B, Hagen G et al (2005) Mater Chem Phys 94:226
29. Santos M, Terezo A, Fernandes V et al (2005) J Solid State Electrochem 9:91
30. Sharma A (1992) Thin Solid Films 208:48
31. Kameyana K, Tsukada K, Yahikozawa K et al (1993) J Electrochem Soc 140(4):956

32. Kameyama K, Tsukada K, Yahikozawa K et al (1994) J Electrochem Soc 141(3):643
33. Pizzini S, Buzzanca G, Mari C et al (1972) Mat Res Bull 7:449
34. Wagner N, Kuhnemund L (1989) Cryst Res Technol 24:1009
35. O'Leary K, Navin T (1974) Chlorine bicenten symposim, vol 30. The Electrochemical Society, San Francisco, pp 174–186
36. Doblhofer D, Metikos M, Ogumi Z et al (1978) Ber Bunsenges Phys Chem 82:1046
37. Lodi G, Srivieri E, Battisti A et al (1978) J Appl Electrochem 8:135
38. Yeo R, Orehotsky J, Visscher W et al (1981) J Electrochem Soc 128:1900
39. Trasatti S (1981) Electrodes of conductive metallic oxides: Part B. Elsevier
40. Hardee K, Kus R (1998) Mod Chlor-Alkali Technol 7:43
41. Ribeiro J, Andrade A (2006) J Electroanal Chem 592:153
42. Iwakura C, Inai M, Manabe M et al (1980) Denki Kagaku 48(2):91
43. Shrivastava P, Moats M (2008) J Electrochem Soc 155(7)